

The Massive Star Population in M101. III. Spectra and Photometry of the Luminous and Variable Stars¹

Skyler H. Grammer², Roberta M. Humphreys² and, Jill Gerke³

ABSTRACT

We discuss moderate resolution spectra, multicolor photometry, and light curves of thirty-one of the most luminous stars and variables in the giant spiral M101. The majority are intermediate A to F-type supergiants. We present new photometry and light curves for three known “irregular blue variables” (V2, V4 and V9) and identify a new candidate. Their spectra and variability confirm that they are LBV candidates and V9 may be in an LBV-like maximum light state or eruption.

Subject headings: galaxies: individual (M101) – supergiants

1. Introduction

Recent supernova surveys have led to the identification of an increasing number of non-terminal optical transients with a wide range of properties. Some of these optical transients appear to be similar to the giant eruptions of the η Car variables (Humphreys et al. 1999; Van Dyk 2005; Van Dyk & Matheson 2012), while others are more akin to the variability of normal Luminous Blue Variables (LBVs). A very small fraction of the optical transients originate from lower luminosity, heavily obscured progenitors that may be extreme asymptotic

¹Based on observations with the Multiple Mirror Telescope, a joint facility of the Smithsonian Institution and the University of Arizona and on observations obtained with the Large Binocular Telescope (LBT), an international collaboration among institutions in the United States, Italy and Germany. LBT Corporation partners are: The University of Arizona on behalf of the Arizona university system; Istituto Nazionale di Astrofisica, Italy; LBT Beteiligungsgesellschaft, Germany, representing the Max-Planck Society, the Astrophysical Institute Potsdam, and Heidelberg University; The Ohio State University, and The Research Corporation, on behalf of The University of Notre Dame, University of Minnesota and University of Virginia.

²Minnesota Institute for Astrophysics, 116 Church St SE, University of Minnesota, Minneapolis, MN 55455, grammer@astro.umn.edu, roberta@umn.edu

³Department of Astronomy, The Ohio State University, 140 West 18th Avenue, Columbus, OH 43210, USA

giant branch (AGB) stars or in a post red supergiant stage of evolution (Thompson et al. 2009; Khan et al. 2010; Bond 2011). The continued monitoring of these optical transients has led to the realization that in some cases the apparent terminal explosion is preceded by smaller eruptions, e.g. SN2005gl (Gal-Yam et al. 2007; Gal-Yam & Leonard 2009), SN2006jc (Pastorello et al. 2007) and most recently the peculiar SN2009ip (Mauerhan et al. 2013; Pastorello et al. 2013; Fraser et al. 2013; Margutti et al. 2013). Consequently, the connection between LBVs, giant eruptions, and true supernovae has come into question. But very little is known about the origin of these giant eruptions, their progenitors and their evolutionary state. An improved census of the most massive, evolved stars including the LBVs, and the hypergiants that occupy the upper HR Diagram is necessary to better characterize the properties of the possible progenitors. For these reasons, we have begun a survey of the evolved massive star populations in several nearby galaxies (Humphreys et al. 2013; Grammer & Humphreys 2013; Humphreys et al. 2014).

This paper is the third in a series on the massive star content of M101. In the first two papers, we presented the photometric analysis and identification of the luminous and massive star populations, here we present spectroscopy and multi-epoch imaging for the most luminous stars. In the next section, we describe our target selection, observations, and data reduction. In §3 we discuss the stars for which we have spectra and light curves, and in §4, we present the light curves for those without spectra. We summarize our conclusions in the last section.

2. Data and Observations

Our motivation for this study is to examine the spectra and photometric variability of the most luminous stars in M101. Using their spectra and light curves, we identify LBV candidates, hypergiants, and other luminous stars and emission-line stars.

2.1. Target Selection

Most of our targets were selected from the Hubble Legacy Archive (HLA) aperture photometry of *HST*/ACS images from proposals GO-9490 (Nov. 2002) and GO-9492 (Jan. 2003) to be brighter than $V \approx 20.5$ mag. Since the images of M101 are crowded, particularly in the spiral arms, we later performed our own photometry using Dolphot (Dolphin 2000) to create a catalog of high precision photometry even in crowded regions (Grammer & Humphreys 2013, hereafter Paper I). In this paper, photometry from Paper I is referred to as the catalog

photometry. We cross-identified targets selected from the HLA with the catalog using a tolerance of $0.1''$ in radial separation. We note that a few of the targets with $V < 20.5$ in the HLA photometry are much fainter in the catalog. The targets with differences in V larger than a few tenths of a magnitude are in regions where aperture photometry is inappropriate (e.g. crowded regions). We visually inspected the surrounding region of each unmatched star and found in all cases, that the unmatched targets were located in parts of the galaxy where photometry was likely to be highly compromised.

In addition to the targets selected from *HST*/ACS photometry, we included blue supergiants and known luminous variables from Sandage & Tammann (1974) and Sandage (1983). The blue supergiants and luminous variables were originally identified on photographic images. Since precise astrometry is required for our study, we used a Sloan Digital Sky Survey (SDSS) g image of M101 to identify the blue supergiants and known variables by eye. Many of the Sandage (1983) stars were also in regions of significant crowding which made positive identification difficult. Thus, we were only able to include 7 stars: B4, B53, B65, B162, V2, V4, and V9.

2.2. Spectroscopy

When we were selecting targets for spectroscopy, we did not yet have the light curves from the Large Binocular Telescope (LBT) survey, discussed below §2.3. Since we could not obtain spectra for every star, we prioritized our targets for spectroscopy by roughly estimating their variability using an “absdiff” image. The absdiff image was created by taking the absolute value of the difference between a reference image, described below, and all other images. Then, the subtracted images were convolved with a 2 pixel Gaussian filter and summed. In the absdiff image, the “brighter” the source, the more variable it is likely to be. All stars with HLA V -band magnitudes brighter than 20.5 mag were then overlaid onto the absdiff image. Priority for spectroscopy was assigned by degree of variability and V -band magnitude. Thus the brightest stars with clear indications of variability received the highest priority. We selected 56 of the brightest and most variable stars for spectroscopy with the Hectospec on the Multiple Mirror Telescope (MMT), and 46 of the fainter ones for spectroscopy with the LBT MODS1 spectrograph. The spectroscopic targets are shown in Figure 1.

The MMT observations were obtained in June 2012 with the Hectospec multi-object spectrometer (MOS; Fabricant et al. 1998). The Hectospec¹ is a fiber-fed MOS with a 1° FOV and 300 fibers; each fiber subtends $1.5''$ on the sky. We used the 600 mm^{-1} grating with the blue tilt centered on 4800\AA and the red tilt centered on 7300\AA . The 600 mm^{-1} grating

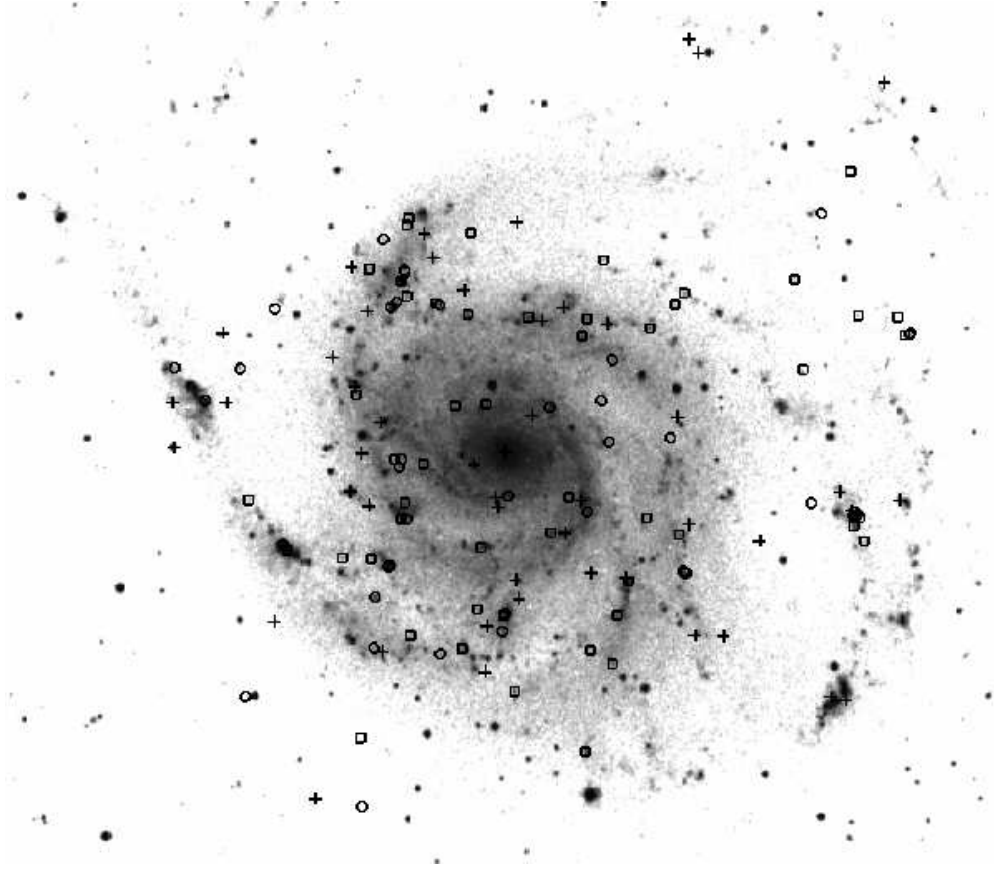


Fig. 1.— POSS II red image of M101. Spectroscopic targets observed with MMT/Hectospec are shown as crosses and LBT/MODS as boxes. Targets without spectra are shown as circles.

gives a spectral coverage of $\sim 2500\text{\AA}$ with $0.54\text{\AA pixel}^{-1}$ resolution. The total integrated exposure times were 240 minutes in the blue and 180 minutes in the red. The spectra were reduced using an exported version of the CfA/SAO SPECROAD package for Hectospec data E-SPECROAD². The spectra were bias subtracted, flat -fielded, wavelength calibrated, and sky subtracted. The IRAF task `sensfunc`, in the *ONEDSPEC* package, was used to flux calibrate the spectra with the standard Feige-66.

The 46 stars selected for observation with the LBT were observed in May 2012 and June 2013 using the Multiple Object Dual Spectrograph (MODS) (Pogge et al. 2006). For multi-object spectroscopy MODS uses masks with a 6.5 arcmin FOV, and a dichroic with two gratings, 400 mm^{-1} and 670 mm^{-1} , to get a full spectral range of 3200\AA to 10000\AA , and moderate resolution ($R \sim 1800$). Since the MODS FOV is considerably smaller than Hectospec, four masks were required to cover the disk of M101. Problems with a beta version of the reduction pipeline prevented us from including the LBT spectra here. Analysis of the LBT/MODS spectra will be included in a future paper.

The 31 confirmed members are listed in order of right ascension in Table 1 with object identification, position, photometry, variability and their spectral type. The 19 foreground stars are in Table 2. The S/N in the spectra for six of the targets was too poor to assign a spectral type. The blue and red spectra of all of the targets are available at <http://etacar.umn.edu/LuminousStars/M101/> in FITS format. The flux calibrated and smoothed spectra are also available in a subdirectory. Spectra of selected members are discussed in the next section.

2.3. LBT Imaging

M101 has been monitored as part of a variability survey of 27 nearby (< 10 Mpc) galaxies using the twin 8.4m LBT (Kochanek et al. 2008; Gerke, Kochanek & Stanek 2014). Between March 2008 and January 2013, M101 was observed using the Large Binocular Camera (LBC) in the *R*-band with the red-optimized LBC-Red camera while simultaneously cycling through observations in the *UBV* filters with the blue-optimized LBC-Blue camera (Giallongo et al. 2008). One of us, J. Gerke, did the basic data reduction steps including overscan correction, bias subtraction, and flat fielding with the IRAF *MSCRED* package, as well as the subsequent analysis of the images. Although M101 was observed even in sub-optimal conditions, only

¹<http://www.cfa.harvard.edu/mmti/hectospec.html>

²External SPECROAD was developed by Juan Cabanela for use on Linux or MacOS X systems outside of CfA. It is available online at <http://iparrizar.mnstate.edu>.

images with a point spread function (PSF) with a full width half max (FWHM) $\lesssim 2''$ are analyzed.

For the variability analysis, the ISIS image subtraction package (Lupton 1998; Alard 2000) was used to process the multiple LBT images. The image subtraction works by matching a reference image to each exposure and subtracting it to leave only the sources which have time-variable flux. The reference image was created by median combining the four best seeing epochs where an epoch is defined as the images for one night. The astrometric solutions were determined using the IRAF package *MSCTPEAK* and SDSS stars (Ivezić et al. 2007) in the FOV. For each epoch, the *R*-band image serves as the astrometric reference image for all four filters which ensures identical astrometric solutions between filters. By doing this, any ambiguity associated with cross-matching sources between filters is minimized. The typical astrometric errors are $0.1''$.

The light curves for the stars with HLA *V*-band magnitudes brighter than 20.5 mag were extracted using ISIS. Instrumental magnitudes for each epoch were converted to *UBVR* magnitudes using photometric calibrations based on SDSS photometry which was transformed from the SDSS *ugriz* filter system to the *UBVR* system using the prescription described by Jordi et al. (2006). The resulting photometry has photometric errors that are $\lesssim 0.06$ magnitudes. For each target, we calculate the root-mean-square (RMS) error, with respect to the median magnitude, as a measure of stellar variability. We identify targets as variable sources for further analysis if their RMS variability is greater than the median photometric error. The *V*-band light curves for spectroscopic targets observed with MMT which met our criterion for variability are shown in Figure 2

3. Classification of the Stars

For discussion, we have grouped the spectra of the confirmed members by their broad spectral characteristics and known variability. In this section we describe the characteristics of four groups: the early-type or hot supergiants, intermediate-type supergiants, emission-line sources, and candidate LBVs. We describe the criteria for membership in each group in the subsections below and discuss the spectra, photometry, and light curves of several interesting or representative stars. Group membership and comments on their spectra and variability are also included in Table 1. For reference, we assume the distance modulus, derived from the tip of the red giant branch, of $(m-M)_0 = 29.05 \pm 0.06(\text{random}) \pm 0.12(\text{systematic})$ magnitudes (Shappee & Stanek 2011). The foreground extinction towards M101 is only $E(B - V) = 0.01$ (Schlegel et al. 1998) which corresponds to a visual extinction of $A_V = 0.03$ magnitudes assuming a Galactic extinction law (Cardelli et al. 1989). For those stars

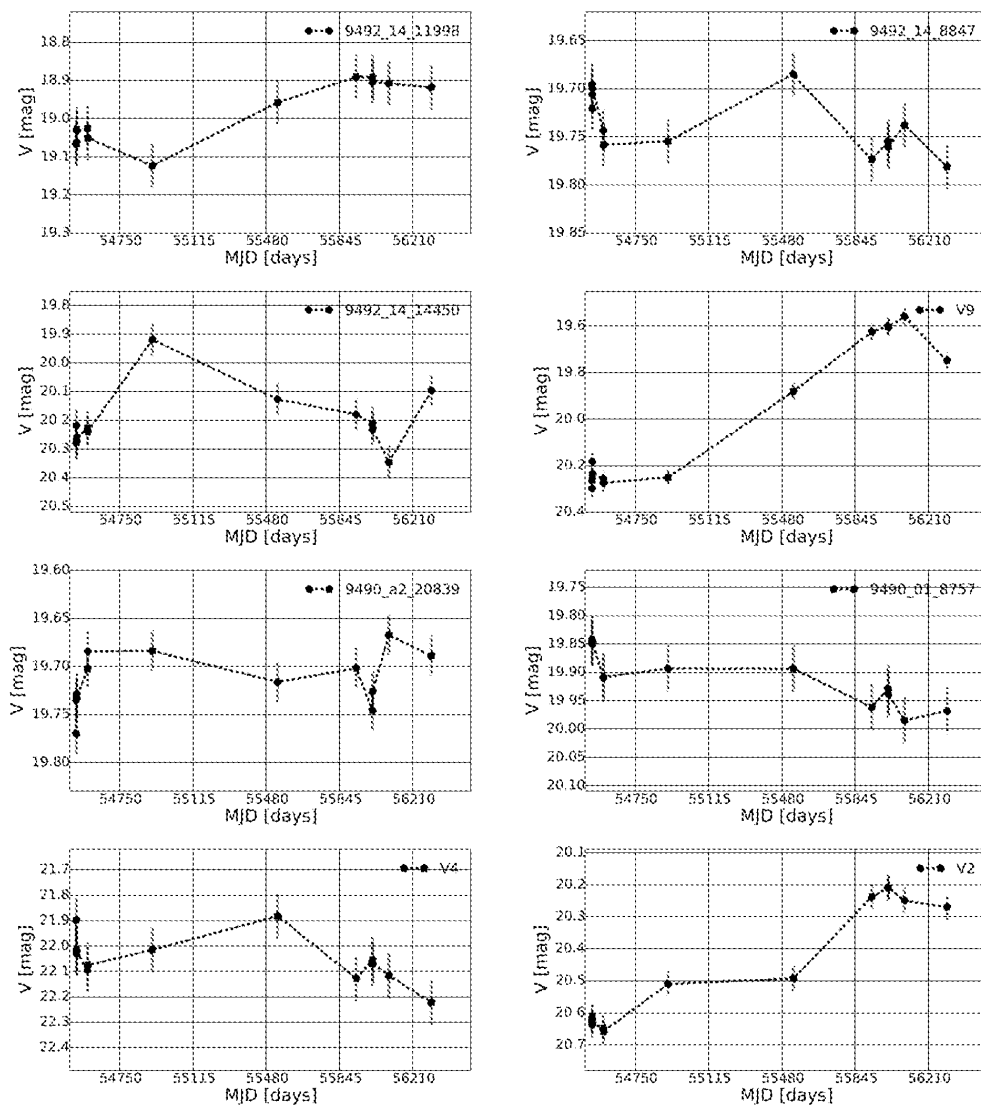


Fig. 2.— The LBT light curves for our stars with spectra that also meet our criterion for variability. Foreground stars are not shown. The x-axis grid lines correspond to 365 days.

with spectral types, we estimate the internal extinction by comparing their observed colors with the intrinsic colors from Flower (1977, 1996, see Table 1). Representative blue spectra from $\approx 3900 - 5200\text{\AA}$ are shown in Figures 3 to 6, and snapshot images of the confirmed members are in the Appendix.

3.1. The Hot Supergiants

This group includes the luminous O- and B-type supergiants. Many of these stars show strong emission lines, mostly nebular, but with an absorption line spectrum strong enough to allow an estimate of the spectral type. In this section we describe stars with interesting spectral features and/or photometric variability.

The spectrum of *9490_02_598* (*early B: I + WN + ?*) shows absorption lines of Si IV $\lambda\lambda 4090$ and 4116 , Si III $\lambda 4552$, C III $\lambda 4650$, and He I $\lambda\lambda 4026$ and 4144 consistent with an early B-type supergiant (Figure 3), although a Ca II K line is also present. The Balmer series, as well as the He I lines of $\lambda\lambda 4471$, 4922 , 6678 and 7065 are in emission with P-Cygni profiles. He I $\lambda 5876$ has a double or split emission profile not present in any of the other emission lines. Emission lines of Fe II, [Fe II], and the broad WN nitrogen emission features at $\lambda 4630-4670\text{\AA}$ and $\lambda 5680-5730\text{\AA}$ are present. The terminal velocity, determined from P-Cygni profiles, is normally measured from the blue edge of the absorption component. Because the spectra are moderate resolution with low S/N, we can more reliably determine the wind velocity from the absorption minima, see (Humphreys et al. 2014). We find a wind velocity of $392.0 \pm 12.6 \text{ kms}^{-1}$ which is on the low end, but in the range for normal early-type supergiants (Crowther et al. 2006; Mokiem et al. 2007).

The catalog photometry for 9490_02_598 is $V = 20.07$ and $(B - V) = 0.30$. Based on its early B-type spectrum, we assume an intrinsic $(B - V)_0$ color of ≈ -0.20 (Flower 1977, 1996) yielding a fairly high interstellar extinction of A_v of 1.6 mag and $M_v = -10.5$ mag. Inspection of the *HST*/ACS *V* band image shows that 9490_02_598 may be a point source although it is located in a crowded region (Figure A10). It was not identified as a point source in the LBT images due to poorer spatial resolution, thus we do not have variability information. The spectrum is similar to an LBV in quiescence (Humphreys & Davidson 1994) but without a light curve we cannot say with any certainty that 9490_02_598 is an LBV candidate. With the Ca II K line it may be composite.

The spectrum of *9490_a3_11594* (*Early B: I + WN:*) is shown in Figure 3. The presence of the C III/O II features at $\lambda\lambda 4068-4076$, Si IV at $\lambda 4089$ and $\lambda 4116$ and absorption lines of He I at $\lambda\lambda 4026$, and 4144 indicate that it has an early B-type spectrum. It also has a weak

WN feature at $\lambda\lambda$ 4630-4670. The relative strength of the O II $\lambda\lambda$ 4070-4076 to He I λ 4026 indicates high luminosity. The emission lines are primarily nebular. We note that $H\beta$, He I λ 5876 and the [O III] lines are double, but the [N II], [S II] and $H\alpha$ in the red are not. These double emission lines are discussed below.

The catalog photometry for 9490_a3_11594 is $V = 21.5$ and $(B - V) = 0.06$, but the HLA and LBT photometry show it ≈ 2 magnitudes brighter and ≈ 0.3 magnitudes redder than the catalog photometry. 9490_a3_11594 is located in a crowded region (Figure A12), thus the magnitudes obtained from aperture photometry may be significantly altered by the neighboring stars. The multi-epoch photometry for 9490_a3_11594 shows no variability in magnitude or color.

9490_a1_7093 (*Mid B: I*) has strong Balmer and nebular emission lines (Figure 3). It resembles 9490_02_598 with He I absorption lines λ 4026, λ 4144, and λ 4387 and the C III/O II absorption feature. These lines suggest an early B-type spectrum, but the Mg II λ 4481 seems too strong. It is in a crowded field so the spectrum may be a blend. We tentatively classify it as a mid-B-type supergiant. Fe II and [Fe II] emission lines are present, as well as the WN nitrogen emission at λ 4630-4670Å. He I λ 5876Å, $H\beta$, the [O III] nebular lines and the Fe II emission lines have double or split emission profiles. However, the nebular [N II] and [S II] lines in the red plus $H\alpha$ do not show the split profiles.

The catalog color and magnitude for 9490_a1_7093 are $(B - V) = 0.31$ and $V = 20.20$, respectively. 9490_a1_7093 is located in a very crowded region (Figure A28) which the lower resolution of the LBT cannot resolve. Consequently, we do not have information on its variability. Since we were unable to assign a precise spectral type to 9490_a1_7093, we estimate the likely extinction for a mid-B type supergiant, $A_V = 1.3$ mag. This may seem high but 9490_a1_7093 is embedded in a region of intense star formation.

B162 (*B8: I*) was identified as a blue supergiant in M101 by Sandage (1983). Followup spectroscopy by Humphreys & Aaronson (1987) confirmed its membership, They estimated its spectral type to be late B to early A, and suggested that B162 may be a composite based on the width of the Balmer lines. Our spectrum of B162 (Figure 3) is one of the few without any nebular contamination. Based on the He I λ 4471 and Mg II λ 4481 absorption lines, we suggest a spectral type of B8; the ratio of Si III λ 4552 to He I λ 4387, as well as the presence of the high luminosity indicator O I λ 7774, confirms that B162 is a supergiant.

The catalog photometry for B162 indicates it is extremely luminous with a V -band magnitude of $V = 19.52$. As a result, B162 is saturated in the LBT images thus preventing us from assessing its variability. Sandage (1983) found no evidence for variability. The observed color for B162 is $(B - V) = 0.09$ which is only 0.1 magnitudes redder than expected

for its spectral type. Correcting for extinction, its M_v is -9.9 mag and with the bolometric correction for a late B-type supergiant, we estimate the bolometric magnitude for B162 to be $M_{bol} = -10.4$. The Balmer lines seem too strong however for such a high luminosity star. It may be a composite or blend of more than one star. See Figure A18, where the object appears to be an unresolved small group of 2 - 3 stars.

Three of the stars described in this subsection have double emission profiles in the nebular and hydrogen emission lines. We find that this is the case for several stars in this study. Since the stars are in crowded regions with strong nebular emission, the double features may be due to emission from the two sides of these large H II regions or from more than one emission region along the line of sight. However in the case of 9490_a1_7093 described above, the Fe II emission lines which presumably arise in the stellar wind, also show the split profiles. For this star the velocity separation of the Fe II peaks is 180 km s^{-1} which corresponds to a possible velocity of expansion of $\approx 90 \text{ km s}^{-1}$.

The spectral types, catalog photometry, visual extinction, and other notes regarding the remaining hot or early-type supergiants are given in Table 1.

3.2. The Intermediate-Type Supergiants

The intermediate supergiant group includes the visually most luminous A- to F-type stars. The intermediate or yellow supergiants, often have strong emission due to stellar winds and mass loss, but due to the degree of nebular contamination in most of these spectra, a stellar origin is uncertain in most cases. Here we discuss some representative and interesting stars in this group.

The spectrum of 9492_14_8847 (F5 I), in Figure 4, shows strong Ca II H and K lines and the luminosity sensitive Fe II/Ti II blends at $\lambda\lambda 4172-4179$. The presence of a weak G-band indicates a spectral type later than $\approx F2$. We estimate 9492_14_8847 to be approximately F5 based on the absorption lines of Ca I $\lambda 4226$, Fe I $\lambda 4046$ and $\lambda 4383$ lines, and Mn I $\lambda 4032$. We were not able to use the Balmer lines in the classification due to strong nebular contamination.

The V -band light curve for 9492_14_8847 (Figure 2) shows only minor variability on the order of ≈ 0.1 magnitudes in amplitude. The catalog photometry for 9492_14_8847 is $V = 19.69$ and $(B - V) = 0.38$. The observed color is only marginally redder than expected, $A_v = 0.2$ and M_v is -9.5 mag. Adopting the bolometric correction for an F5 supergiant (BC = 0.18; Flower 1977, 1996), its bolometric luminosity of 9492_14_8847 is $M_{bol} = -9.3$. Furthermore, the *HST*/ACS V image shows that 9492_14_8847 is on the periphery of a star-forming region

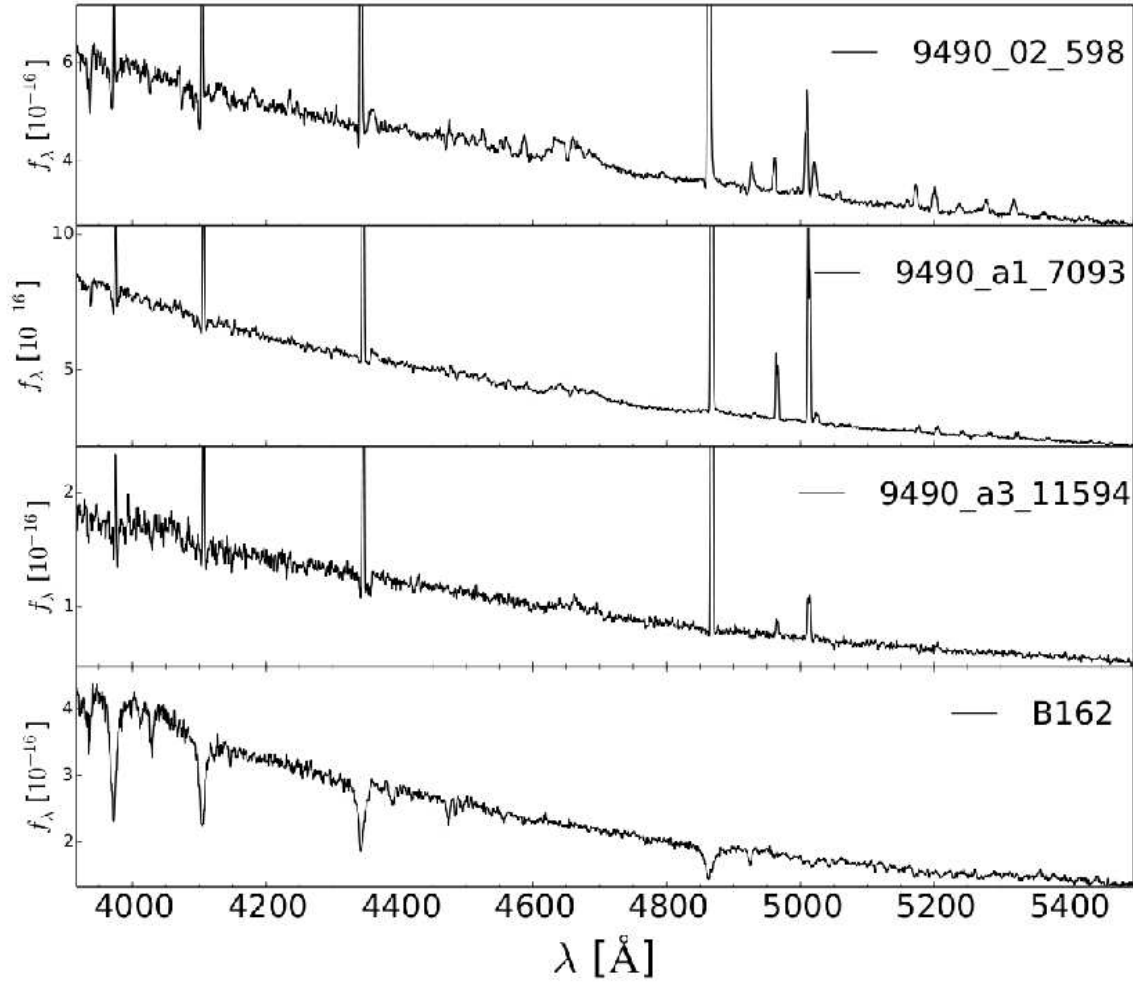


Fig. 3.— Spectra of selected early-type supergiants. The spectra are flux calibrated and smoothed with a 3 box smooth in the *splot* task in IRAF.

(Figure A2) but appears to be a single point source. Thus, we conclude that 9492_14_8847 is an intermediate supergiant which occupies the same part of the HR diagram as the yellow supergiants in M31 and M33 (Humphreys et al. 2014).

The low S/N spectrum of *9492_14_14450 (Early A I)* in Figure 4 shows emission lines of Fe II and [Fe II] and strong H α and H β emission with broad wings asymmetric to the red, indicative of Thompson scattering and the presence of a stellar wind. The relative strength of He I λ 4471 and Mg II λ 4481, suggest an early A spectral type. The [O III] lines and He I λ 5876 are double, and λ 5876 also has a P Cyg profile. While H β and H γ are not clearly double-peaked, they are both asymmetric to the red.

Based on the catalog photometry, 9492_14_14450 had an apparent magnitude of $V = 19.74$ and an observed color of $(B - V) = 0.34$ in January 2003. The multi-epoch photometry from the LBT shows variability on the order of ≈ 0.4 magnitudes (Figure 2) with a maximum of $V = 19.95$ in March 2009 (MJD 54912). 9492_14_14450 is located in a very crowded, star forming region (Figure A3), and based on its observed color has relatively high interstellar extinction, $A_v = 0.9$ mag, assuming an A2 spectral type. M_v is ≈ -10.2 mag and M_{bol} is -10.3 . Thus 9492_14_14450 has several characteristics of a stellar wind and given its high luminosity based on its catalog photometry, it qualifies as a warm hypergiant star possibly similar to those in M31 and M33 (Humphreys et al. 2013).

9490_03_6943 has an early to mid-A-type spectrum.. It is one of the few targets with no nebular contamination (Figure 4). Its strong H α emission line with very broad wings and P Cygni absorption is thus circumstellar. It is relatively isolated (Figure A15) and appears to be a single star. The catalog photometry is not contaminated and gives rather low visual extinction for a mid A spectral type (\sim A2-A5) and $M_v = -9.0$.

The catalog photometry, visual extinction, spectral types, and any other notes regarding the remaining intermediate-type supergiants are given in Table 1.

3.3. Emission-Line Sources

The emission-line stars have a blue continuum and strong emission lines. The distinction between targets in this group and the hot supergiants is the lack of absorption features permitting the estimation of a spectral type. There are only three stars in this group and one appears to be an H II region.

The spectrum of *9490_a3_10940(Of/WN)* is dominated by strong H and He I emission as well as the broad N III and N II emission features seen in WN stars (Figure 5). Some

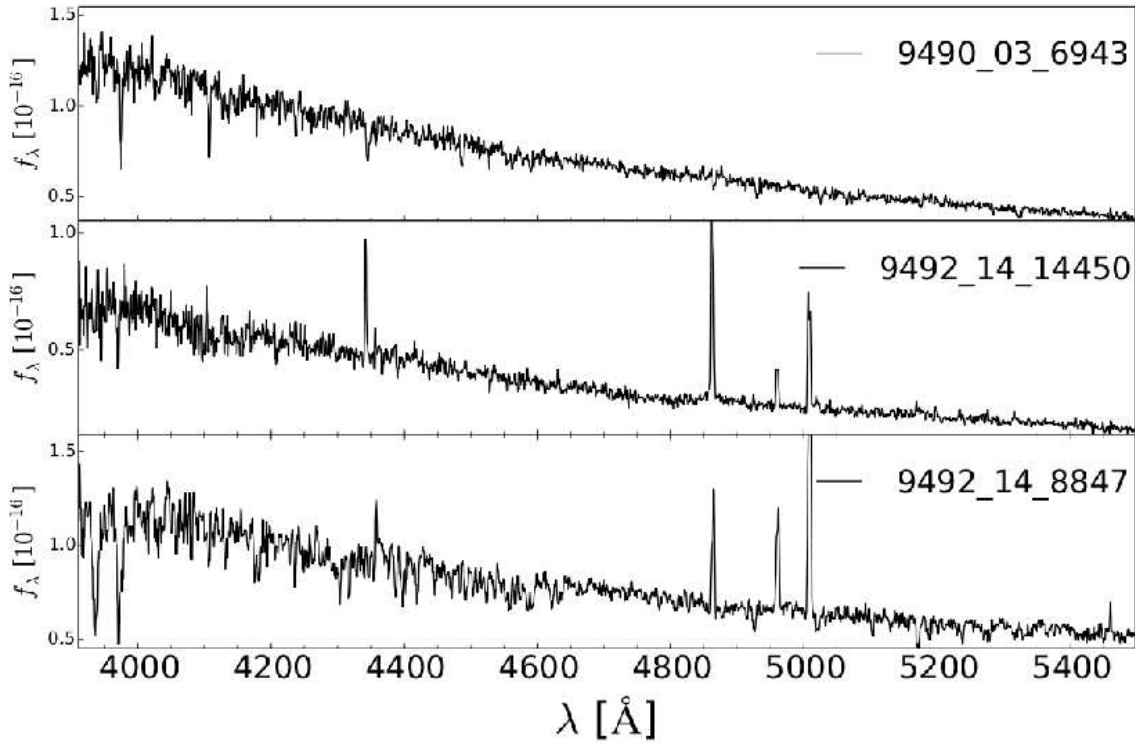


Fig. 4.— Spectra of selected intermediate-type supergiants. The spectra are flux calibrated and smoothed with a 3 box smooth in the *splot* task in IRAF.

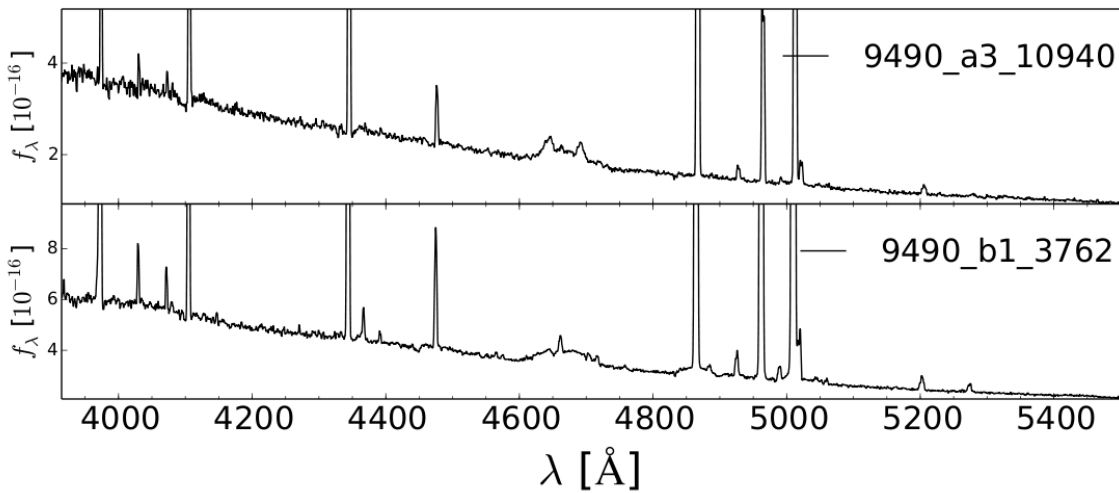


Fig. 5.— Spectra of the two emission line stars. The spectra are flux calibrated and smoothed with a 3 box smooth in the *splot* task in IRAF.

of the weaker emission lines include He II $\lambda 4686$, O II $\lambda\lambda 4070-4076$, and Fe II. Based on its spectral features, 9490_a3_10940 is an Of/WN star. The catalog magnitude for 9490_a3_10940 is $V = 21.49$ which is much fainter than our cutoff of $V \lesssim 20.5$ based on HLA photometry. Inspection of the V -band ACS image (Figure A7) shows that 9490_a3_10940 is in a crowded region and the HLA aperture photometry is contaminated by nearby stars. The observed color is $(B - V) = -0.06$ which is approximately 0.2 magnitudes redder than we would expect for a star as hot as 9490_a3_10940. Though we do not have a precise spectral type for 9490_a3_10940, adopting $(B - V) \approx -0.3$ mag, which is typical for hot O-type stars, the extinction towards 9490_a3_10940 is roughly 0.7-0.8 magnitudes and M_v is -8.3 mag. Correcting for extinction and adopting a bolometric correction of -3.0, we estimate the bolometric luminosity to be $M_{bol} \approx -11.3$.

9490_b1_3762 is in the giant star-forming complex NGC 5461 (Figure A30) and many of the emission features in its spectrum (Figure 5) are nebular. Despite the strong nebular contamination, the $H\alpha$ and $H\beta$ line profiles have very broad wings suggesting a strong stellar wind. We also identify He I, C III $\lambda\lambda 4647-4652$, and C IV $\lambda 4658$ weak absorption lines indicating an underlying hot star. Emission lines of [S II] Fe II, [Fe II], and [Fe III] and broad WN nitrogen emission region from 4620 - 4720Å are present. As in several other stars, $H\beta$, the [O III] lines and He I $\lambda 5876$ have split emission profiles.

The catalog photometry for 9490_b1_3762 gives $V = 22.13$ and $(B - V) = 0.23$. The emission lines from the highly-ionized species we see in the spectrum can only be produced by the radiation from an OB-type star with $(B - V) < 0$. Since the observed color is much redder than we expect for an OB-type star, it is likely that 9490_b1_3762 is highly reddened or a blend of objects. Since it is in such a highly crowded region (Figure A30) we cannot determine its variability from the LBT images.

The low S/N spectrum of $B4$ (Sandage 1983) has the emission line spectrum of an H II region. $H\beta$, He I $\lambda 5876$, and the [O III] lines show split or double profiles.

3.4. Candidate LBVs

A census of variable stars in M101 was first conducted by Sandage & Tammann (1974) who identified nine irregular blue variables (V1 - V9). Subsequent photometric studies confirmed the variable nature of V1 and V2, and added a tenth star (V10; Sandage 1983). Fifty-year historical light curves for the candidate LBVs V1, V2, and V10 are presented in Sandage (1983). V3 through V9 are known to be variable, and are considered to be candidate LBVs, but lack historical light curves. Here we present the light curves and spectra for V2,

V4, and V9. We have also identified an additional candidate LBV, 9492_14_11998.

The spectrum of 9492_14_11998 shown in Figure 6 is dominated by Balmer and He I emission lines with strong P-Cygni profiles. The line profiles of $H\alpha$ and $H\beta$ have very broad wings and are asymmetric to the red, a feature characteristic of Thompson scattering. We estimate a wind velocity of $369 \pm 9 \text{ km s}^{-1}$ from the P Cygni absorption component in the hydrogen and He I emission lines. This is somewhat higher than the wind velocities of the M31 and M33 LBVs measured the same way (Humphreys et al. 2014), but on the low end for normal OB supergiants (Crowther et al. 2006; Mokiem et al. 2007). Weak Fe II emission is also present. We also identify absorption lines of He I at $\lambda\lambda 4009, 4026, 4121$ and 4144\AA , and Si II at $\lambda 4128\text{-}31\text{\AA}$ typical of an early B2-B3-type supergiant

The V -band light curve for 9492_14_11998 in Figure 2 shows that the star has steadily increased in brightness by approximately 0.2 magnitudes over the last 4 years. The spectrum for 9492_14_11998 was obtained at its current visual maximum of 18.9 mag. The catalog photometry, which was observed in January 2003, indicates that 9492_14_11998 had a significantly fainter apparent magnitude ($V = 19.40$) than its present value. Its observed color in 2003 was $(B - V) = 0.19$ and based on our LBT photometry, it has not changed.

If we assume an intrinsic color of $(B - V)_0 \approx -0.1$ corresponding to a mid-B-type supergiant (Flower 1977, 1996) and a Galactic extinction curve, the visual extinction is $A_V \approx 0.9$ magnitudes. Correcting the *HST*/ACS visual magnitude for this extinction, 9492_14_11998 has an absolute visual magnitude of $M_V = -10.55$ magnitudes. Adopting the bolometric correction (BC) for a mid-B supergiant ($BC \approx -1.05$; Flower 1977, 1996), 9492_14_11998 has a high bolometric luminosity of $M_{bol} = -11.6$, but inspection of the *HST*/ACS V image (Figure A1) shows that it is in a crowded region and the photometry is likely contaminated by neighboring stars. Despite the photometric uncertainties introduced by crowding, the spectral features of 9492_14_11998 are similar to an LBV in quiescence. Continued monitoring will be necessary to determine whether or not 9492_14_11998 is an LBV.

V2 is one of the three previously identified LBV candidates in M101 (Sandage 1983). Humphreys & Aaronson (1987) describe its spectrum as having $H\alpha$, $H\beta$, [O II] $\lambda 3727$, and Fe II in emission. Our higher S/N spectrum confirms the described features and reveals broad-winged $H\alpha$ and $H\beta$ emission lines, as well as [N II], and [S II] in emission in the red. $H\beta$ and the Fe II emission lines redward of $H\beta$ have split-emission-line profiles. These characteristics along with the fact that there is no [O III] $\lambda 4959$ and $\lambda 5007$ in emission suggests that the [N II], and [S II] lines may originate in the circumstellar environment rather than a nearby H II region. Furthermore, the *HST*/ACS V -band image (Figure A29) shows that V2 is a single star and there is no indication of an H II region within the fiber.

The 50-year historical light curve for V2 is shown in Sandage (1983). Over the 50 years it was monitored, V2 faded from $V \approx 19.1$ in 1910 to $V \approx 20.3$ in 1960. Our 4.5-year V -band light curve (Figure 2) indicates that V2 is increasing in brightness from $V = 20.6$ in 2008 to $V = 20.25$ in 2013. The current spectrum shows V2 to be a hot star and, therefore, in quiescence if it is an LBV.

The spectrum of V4 is shown in Figure 6 and is fairly noisy despite smoothing. It is dominated by strong H, He I, [N II], and [S II] emission lines. The spectrum of V4 also shows Fe II emission throughout, although the lines are not particularly strong.

Although V4 was originally identified as a variable star in M101, (Sandage & Tammann 1974), there is no historical light curve. The LBT light curve for V4 displays variability with an amplitude of approximately 0.4 magnitudes in the V -band (Figure 2) with a maximum magnitude of $V = 21.9$. The catalog photometry from observations obtained in 2003 show V4 to be at $V = 22.0$. Sandage & Tammann (1974) list the visual minimum and maximum for V4 to be $V = 22.2$ and $V = 19.9$, respectively. Assuming their photometry to be accurate, V4 is currently at its visual minimum and the oscillations we see are likely the low-amplitude variations commonly superposed on the longer time scale LBV minima and maxima.

The spectrum of V9 in Figure 6 shows strong Balmer emission. The $H\beta$ and $H\alpha$ lines have broad, asymmetric wings indicating a strong stellar wind. We do not see any indication of P-Cygni profiles, however, this could be due to the large amount of nebular contamination filling in the absorption lines. Absorption lines of Fe II, Mg II $\lambda 4481$, and the Ca II K-line are present. The luminosity sensitive O I $\lambda 7774$ in intermediate type stars is also present. V9 is located on the periphery of a large star-forming complex which is not within the *HST*/ACS footprint. However, we have examined the LBT images (Figure A4) and although the complex is not resolved, V9 is located far enough away that its spectrum and photometry should not be seriously contaminated, and it is unlikely that the spectrum is a blend

The LBT V -band light curve for V9 indicates that the star has increased in visual brightness by approximately 0.8 magnitudes over the last 4 years from $V = 20.2$ in 2008 to $V = 19.6$ in 2012. The most recent data suggest V9 may be fading again. Similar to V4, V9 was originally identified as a variable star in M101 (Sandage & Tammann 1974) with similar minima and maxima: $V_{min} = 20.3$ (1950) and $V_{max} = 19.5$ (1927/1947). When the Hectospec spectrum was observed, V9 was near its visual maximum based on the LBT light curve (Figure 2). Although dominated by a strong continuum and Balmer emission, its spectrum suggests that the underlying star was an early A-type supergiant and therefore may be an LBV in its optically thick wind or visual maximum state. Given its spectrum and variability history, it is very likely that V9 is an LBV.

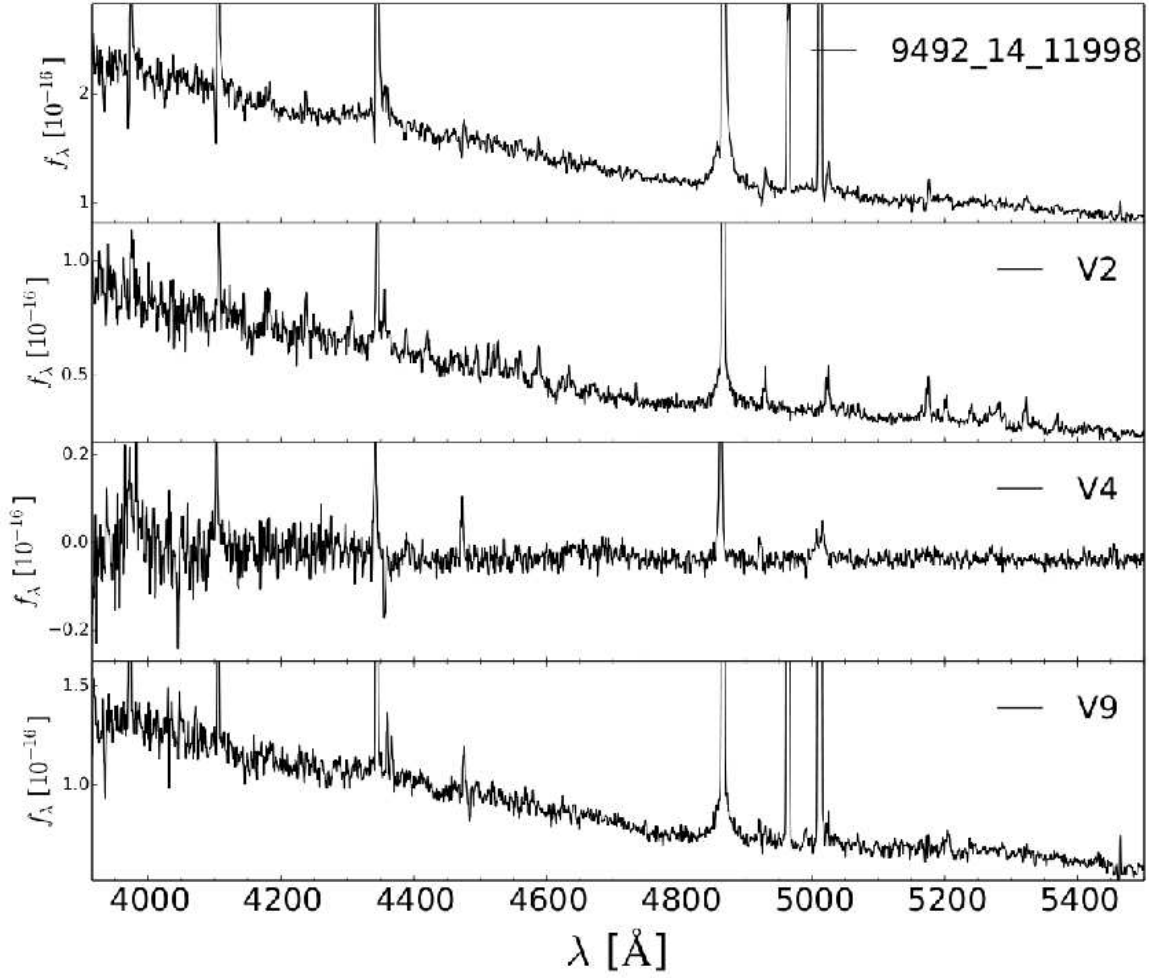


Fig. 6.— Spectra of the four LBV candidates. The spectra are flux calibrated and smoothed with a 3 box smooth in the *splot* task in IRAF.

4. The Variables Without Spectra

In this section, we discuss the light curves for the targets without spectra that met our criterion for variability. We separate the variables by their photometry into three groups: hot or early-type (O–B), intermediate (A–F), and cool (G–M) stars. Assuming zero reddening, the selection criteria for our groups corresponds to $(B - V) < 0$, $0 < (B - V) < 0.9$, and $(B - V) > 0.9$, respectively. Based on our estimates of A_V for our spectroscopically confirmed members (Table 1), the majority of the stars are likely to be at least somewhat reddened. Therefore, we have relaxed our selection criteria to: hot $[(B - V) \leq 0.2]$, intermediate $[0.2 < (B - V) < 1.0]$, and cool $[(B - V) > 1.0]$. When available, we used the *HST*/ACS catalog photometry to assign the stars to the three groups. For targets that were not recovered in the catalog, we used the LBT photometry, although the LBT colors are unlikely to be precise in crowded regions.

We have LBT spectra for many of the stars in this section. When the improved reduction pipeline is complete, we will discuss the spectra along with their light curves in a future paper.

4.1. Early-Type Variables

Figure 7 shows the *V*-band light curves for the eight early-type variables. The majority have photometric variability on the order of a few tenths of a magnitude. Two of the stars, 9492_10_SF89 and 9492_12_961, show changes in *V*-band that are ≈ 1 magnitude. In both cases, the stars are fading. In 2003, they had *V*-band magnitudes of $V = 21.22$ and $V = 20.94$, respectively, measured from the *HST*/ACS images. In March 2008, the LBT *V*-band magnitudes did not differ by more than a tenth of a magnitude compared to 2003. Though we do not have data between 2003 and 2008, the similarities suggest that their decline in brightness may be a recent development or alternatively the stars may be semi-periodic. Given their photometric colors and variability, 9492_10_SF89 and 9492_12_961 may also be LBVs. Spectral analysis and photometric monitoring will be necessary for confirmation.

4.2. Intermediate-Type Variables

The *V*-band light curves for the six variables with $0.2 < (B - V) \leq 1.0$ are shown in Figure 8. Our color criteria for the intermediate group could include supergiant Cepheids. To ensure that we have not re-identified any known Cepheids, we have cross-referenced the astrometry of the intermediate variables with the Shappee & Stanek (2011) catalog of M101 Cepheids and removed any matches.

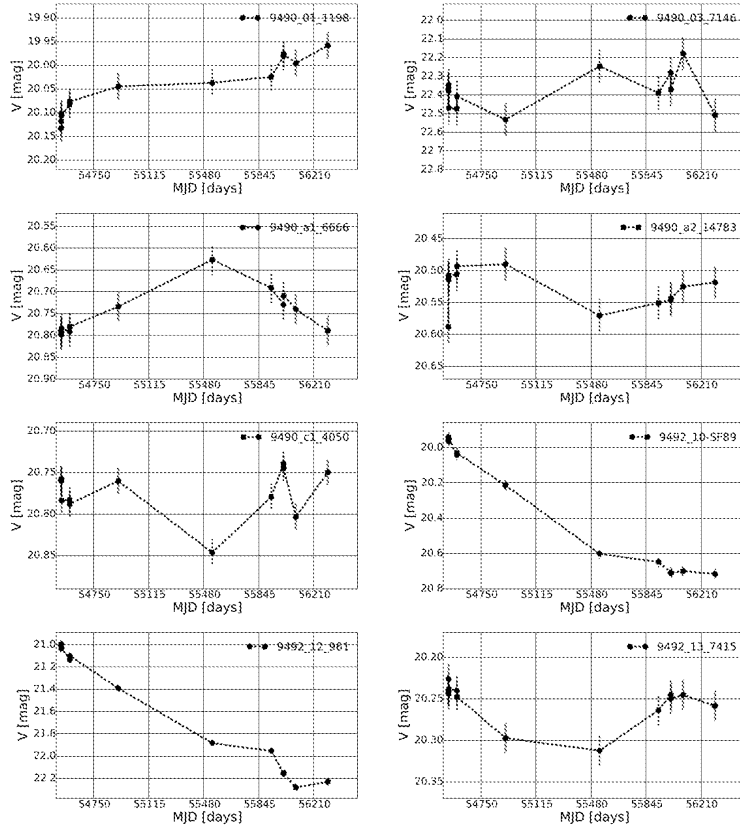


Fig. 7.— The V-band light curves for the early-type variables (i.e. targets that meet our criterion for variability and have $(B - V) \leq 0.2$). The x-axis grid lines represent 365 days.

The intermediate-type variables have photometric properties that overlap with the intermediate type supergiants and with LBVs at maximum light (Humphreys & Davidson 1994). It is typical for A to F supergiants to exhibit variability on the order 0.1 – 0.2 magnitudes known as α Cygni variability (van Genderen & Sterken 2002). LBVs can also exhibit α Cygni variability, during an extended maximum, but with a higher amplitude (± 0.5 magnitudes; van Genderen et al. 1997b,a). The variables presented here primarily exhibit α Cygni variability typical of intermediate-type supergiants. However, 9492_13_6986 and 9492_13_11163 show larger amplitude variability on the order of ≈ 0.5 magnitudes. Furthermore, 9492_13_11163 was brighter by 0.5 magnitudes in January 2003 from the *HST*/ACS catalog photometry compared with the March 2008 LBT *V*-band magnitude. Without a spectrum, we cannot say with any certainty that these stars are not typical intermediate-type supergiants, however, their variability suggests they could be LBVs. Followup observations will be necessary for confirmation.

4.3. Cool Variables

Finally, we present the *V*-band light curves (Figure 9) for the six stars which meet our variability criterion and have $(B - V) > 1.0$. This group very likely includes red supergiants and foreground K and M dwarfs. The stars in this group exhibit variability in the *V*-band that is 0.2 – 0.4 magnitudes in amplitude which is typical of K and M supergiants (Meynet et al. 2011, and references therein), but based on the analysis of Grammer & Humphreys (2013), it is likely that a large fraction of the cool variables are foreground. We present the light curves here, but defer the analysis to a future paper which will include the spectra.

5. Summary and Future Work

In this third paper on our survey of the massive star population in M101, we present the results of spectral classification and multicolor photometry of 50 of the visually brightest stars in the field and confirm that 31 are members of M101. It is not surprising that the majority are intermediate-type supergiants with A to F-type spectra since we selected the targets based on their visual apparent magnitude and variability. We present new photometry and light curves for three candidate LBVs, V2, V4 and V9 and identify a new candidate, 9492_14_11998. Their spectra and variability confirm that they are LBV candidates and V9 may be in an LBV-like maximum light state or eruption. Followup spectra and continued photometric monitoring of these candidates will be necessary for confirmation and to deter-

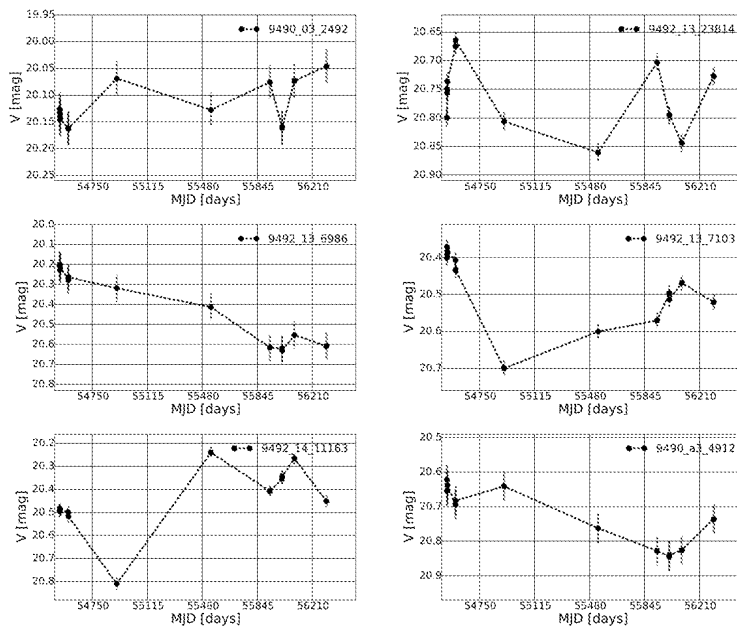


Fig. 8.— The V -band light curves for the intermediate-type variables (i.e. targets that meet our criterion for variability and have $0.2 < (B - V) \leq 1.0$). The x-axis grid lines represent 365 days.

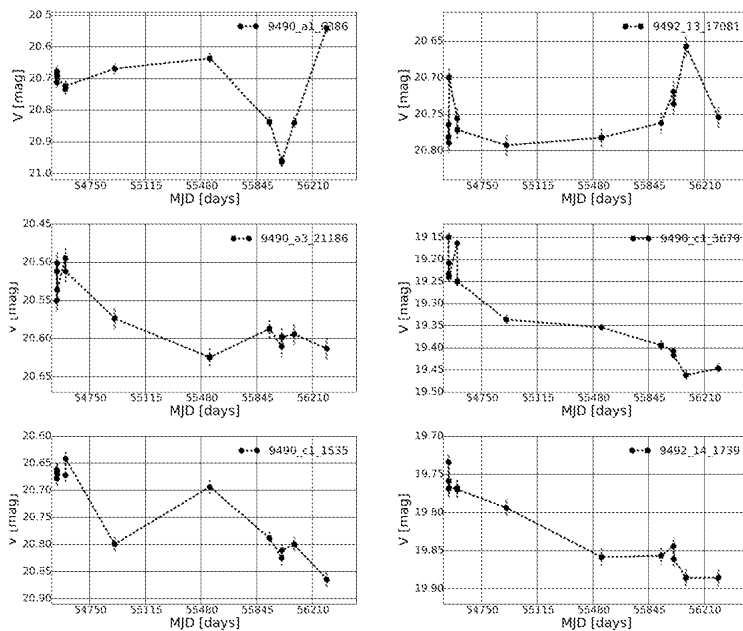


Fig. 9.— The V -band light curves for the cool variables (i.e. targets that meet our criterion for variability and have $(B - V) > 1.0$). The x-axis grid lines represent 365 days.

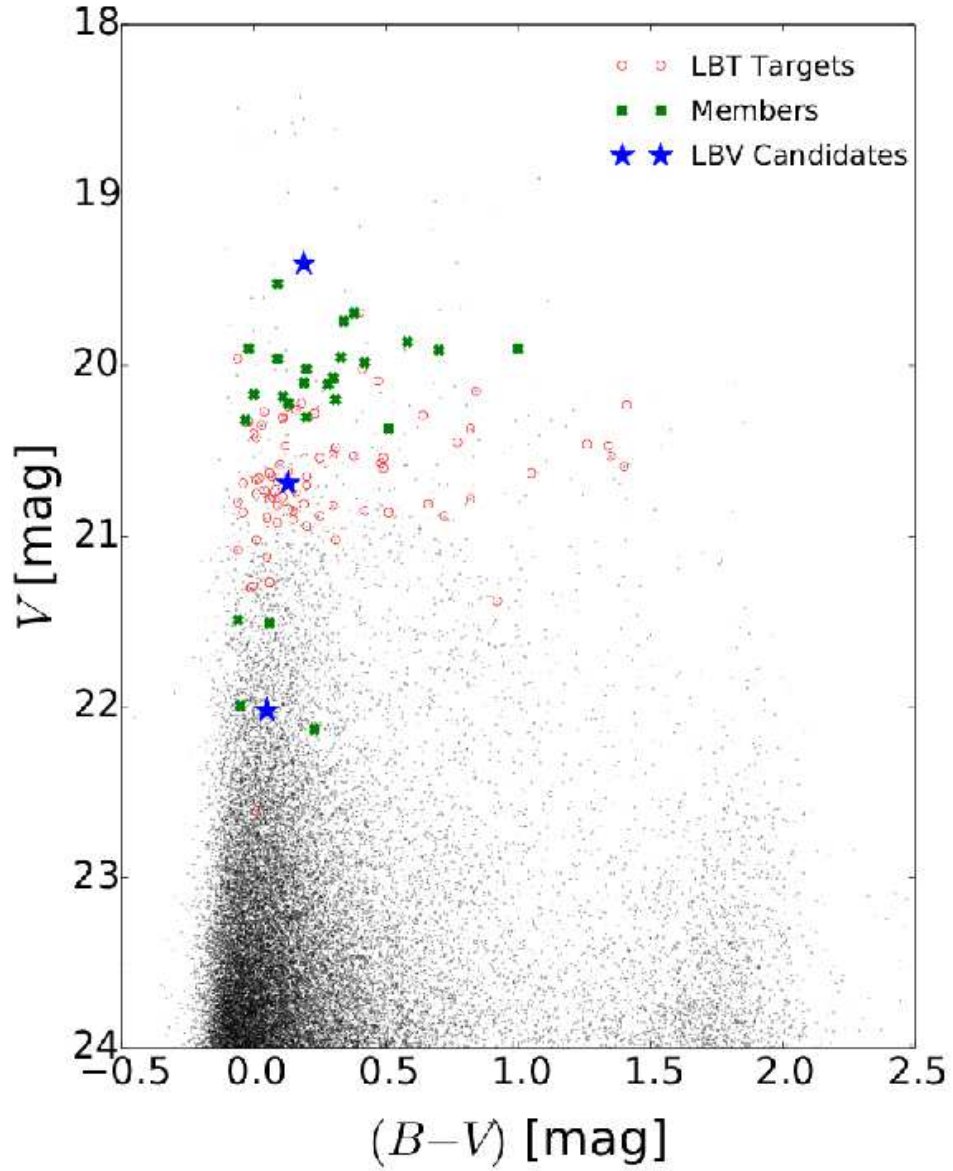


Fig. 10.— The color-magnitude diagram from Paper I showing the confirmed members, the LBVs, and the LBT targets. Confirmed non-members have been removed.

mine the nature of their observed variability. We also discuss the light curves of 20 variables that lack spectroscopy. Four of these stars with large amplitude variability may be LBV candidates.

Figure 10 shows the observed color-magnitude diagram from Paper I with the confirmed members identified. The LBV candidates and the targets observe with the LBT are identified separately and the non-members have been removed.

Forty-six additional stars have been observed with the LBT/MODS. When the LBT/MODS reduction pipeline is completed, the addition of these stars including many of the variables will allow a more complete sampling of the upper HR Diagram in M101.

Research by R. Humphreys and S. Grammer on massive stars is supported by the National Science Foundation grant AST-1109394. Based on observations made with the NASA/ESA Hubble Space Telescope, and obtained from the Hubble Legacy Archive, which is a collaboration between the Space Telescope Science Institute (STScI/NASA), the Space Telescope European Coordinating Facility (ST-ECF/ESA) and the Canadian Astronomy Data Centre (CADC/NRC/CSA).

Facilities: MMT/Hectospec, LBT/LBC, HST/ACS

A. Snapshot images

Snapshot images of 30 of the confirmed members from the *HST*/ACS F555W frame are shown here with a $1''.5$ diameter circle equal to the Hectospec aperture. At the distance of M101, this is 47 pc. The images are displayed in the same order as the stars in Table 1. There is no image for B4. The snapshots are displayed here in pairs to save space. In the published on-line paper they will be separate and interested readers will be able to click on each for an enlarged view.



Fig. A1,2.— a. 9492_14_11998 b. 9492_14_8847

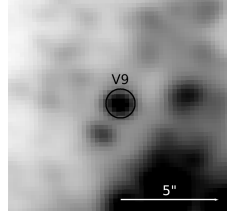
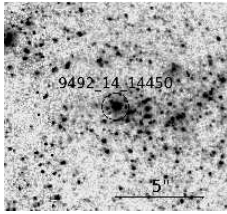


Fig. A3,4.— a. 9492_14_14450 b. V9, an LBV candidate, LBT image.

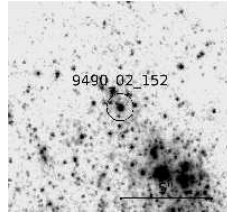
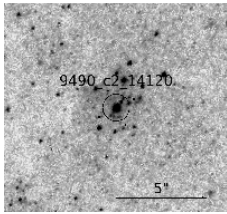


Fig. A5,6.— a. 9490_c2_14120 b. 9490_02_152

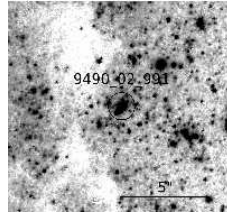
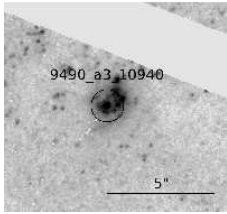


Fig. A7,8.— a. 9490_a3_10940 b. 9490_02_991

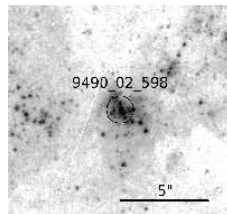
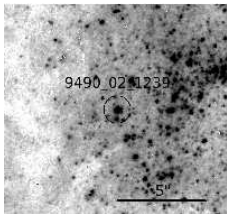


Fig. A9,10.— a. 9490_02_1239 b. 9490_02_598

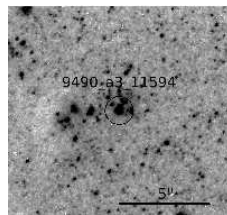
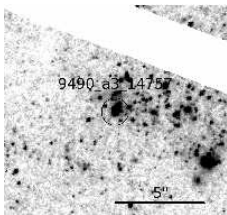


Fig. A11,12.— a. 9490_a3_14757 b. 9490_a3_11594

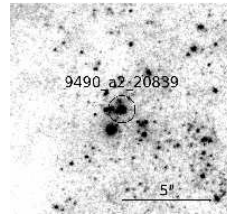
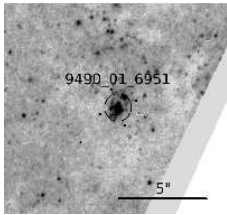


Fig. A13,14.— a. 9490_01_6951 b. 9490_a2_20839

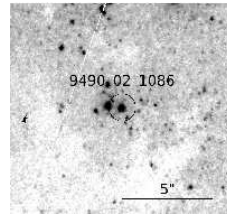
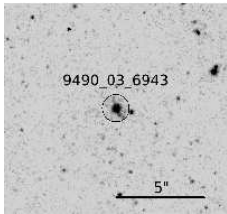


Fig. A15,16.— a. 9490_03_6943 b. 9490_02_1086

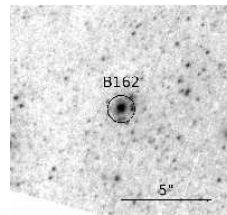
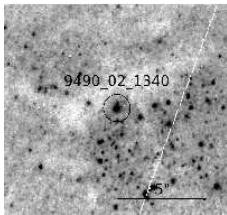


Fig. A17,18.— a. 9490_02_1340 b. B162

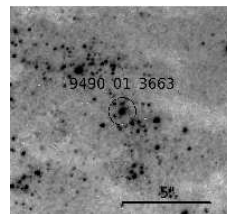
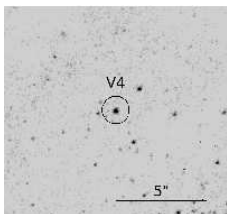


Fig. A19,20.— a. V4, an LBV candidate. b. 9490_01_3663

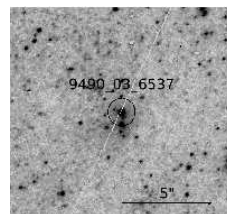
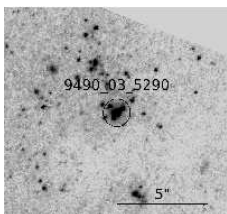


Fig. A21,22.— a. 9490_03_5290 b. 9490_03_6537

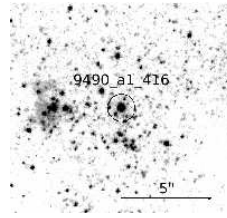
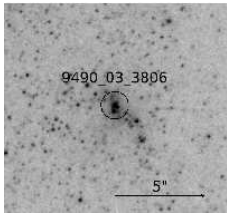


Fig. A23,24.— a. 9490_03_3806 b. 9490_a1_416

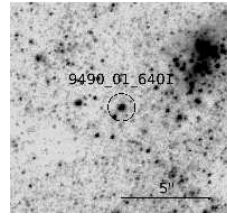
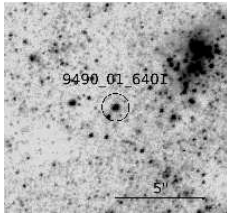


Fig. A25,26.— a. 9490_a1_6401 b. 9490_03_1487

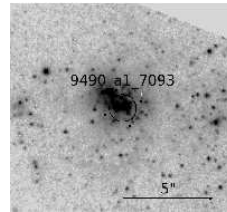
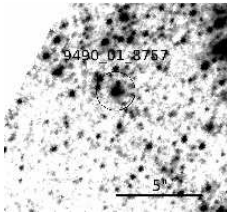


Fig. A27,28.— a. 9490_01_8757 b. 9490_a1_7093

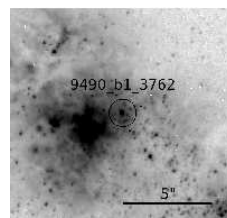
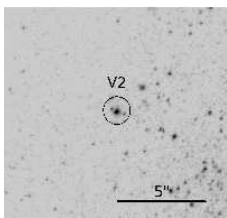


Fig. A29,30.— a. V2, an LBV candidate. b. 9490_b1_3762

REFERENCES

- Alard, C. 2000, *A&AS*, 144, 363
- Bond, H. E. 2011, *ApJ*, 737, 17
- Cardelli, J. A., Clayton, G. C., & Mathis, J. S. 1989, *ApJ*, 345, 245
- Crowther, P. A., Lennon, D. J., & Walborn, N. R. 2006, *A&A*, 446, 279
- Dolphin, A. E. 2000, *PASP*, 112, 1383
- Fabricant, D. G., Fata, R. G., & Epps, H. W. 1998, in *Society of Photo-Optical Instrumentation Engineers (SPIE) Conference Series*, Vol. 3355, *Optical Astronomical Instrumentation*, ed. S. D’Odorico, 232–241
- Flower, P. J. 1977, *A&A*, 54, 31
- Flower, P. J. 1996, *ApJ*, 469, 355
- Fraser, M., et al. 2013, *MNRAS*, 433, 1312
- Gal-Yam, A. & Leonard, D. C. 2009, *Nature*, 458, 865
- Gal-Yam, A., et al. 2007, *ApJ*, 656, 37
- Gerke, J. R., Kochanek, C. S. & Stanek, K. Z. 2014, *MNRAS*, submitted
- Giallongo, E., et al. 2008, *A&A*, 482, 349
- Grammer, S., & Humphreys, R. M. 2013, *AJ*, 146, 114
- Humphreys, R. M., & Aaronson, M. 1987, *AJ*, 94, 1156
- Humphreys, R. M., & Davidson, K. 1994, *PASP*, 106, 1025
- Humphreys, R. M., Davidson, K., Grammer, S., Kneeland, N., Martin, J. C., Weis, K., & Burggraf, B. 2013, *ApJ*, 773, 46
- Humphreys, R. M., Davidson, K., & Smith, N. 1999, *PASP*, 111, 1124
- Humphreys, R. M., Weis, K., Davidson, K., Bomans, D. J., & Burggraf, B. 2014, *ApJ*, 790, 48
- Ivezić, Ž., et al. 2007, *AJ*, 134, 973

- Jordi, K., Grebel, E. K., & Ammon, K. 2006, *A&A*, 460, 339
- Khan, R., Stanek, K. Z., Prieto, J. L., Kochanek, C. S., Thompson, T. A., & Beacom, J. F. 2010, *ApJ*, 715, 1094
- Kochanek, C. S., Beacom, J. F., Kistler, M. D., Prieto, J. L., Stanek, K. Z., Thompson, T. A., & Yüksel, H. 2008, *ApJ*, 684, 1336
- Lupton, W. 1998, in *Society of Photo-Optical Instrumentation Engineers (SPIE) Conference Series*, Vol. 3351, *Telescope Control Systems III*, ed. H. Lewis, 210–221
- Margutti, R., et al. 2013, *ArXiv e-prints*
- Mauerhan, J. C., et al. 2013, *MNRAS*, 430, 1801
- Meynet, G., Georgy, C., Hirschi, R., Maeder, A., Massey, P., Przybilla, N., & Nieva, M.-F. 2011, *Bulletin de la Societe Royale des Sciences de Liege*, 80, 266
- Mokiem, M. R., et al. 2007, *A&A*, 465, 1003
- Pastorello, A., et al. 2007, *Nature*, 447, 829
- Pastorello, A., et al. 2013, *ApJ*, 767, 1
- Pogge, R. W., et al. 2006, in *Society of Photo-Optical Instrumentation Engineers (SPIE) Conference Series*, Vol. 6269, *Society of Photo-Optical Instrumentation Engineers (SPIE) Conference Series*
- Sandage, A. 1983, *AJ*, 88, 1569
- Sandage, A., & Tammann, G. A. 1974, *ApJ*, 194, 223
- Schlegel, D. J., Finkbeiner, D. P., & Davis, M. 1998, *ApJ*, 500, 525
- Shappee, B. J., & Stanek, K. Z. 2011, *ApJ*, 733, 124
- Thompson, T. A., Prieto, J. L., Stanek, K. Z., Kistler, M. D., Beacom, J. F., & Kochanek, C. S. 2009, *ApJ*, 705, 1364
- Van Dyk, S. D. 2005, in *Astronomical Society of the Pacific Conference Series*, Vol. 332, *The Fate of the Most Massive Stars*, ed. R. Humphreys & K. Stanek, 47
- Van Dyk, S. D., & Matheson, T. 2012, in *Astrophysics and Space Science Library*, Vol. 384, *Eta Carinae and the Supernova Impostors*, ed. K. Davidson & R. M. Humphreys, 249

van Genderen, A. M., de Groot, M., & Sterken, C. 1997a, A&AS, 124, 517

van Genderen, A. M., & Sterken, C. 2002, A&A, 386, 926

van Genderen, A. M., Sterken, C., & de Groot, M. 1997b, A&A, 318, 81

Table 1. Members of M101

Catalog ID	Star ID	α_{J2000}	δ_{J2000}	V	$(B - V)$	Group	Variability	A_V	Comments
J140220.98+542004.38	9492_14_11998	14:02:20.98	54:20:04.38	19.40	0.19	LBV Cand.	BVR	0.9	P-Cyg H, He I; Fe II em.; see text, Figure 6
J140227.30+541952.50	9492_14_8847	14:02:27.30	54:19:52.50	19.69	0.38	Im. SG	BVR	0.2	F5 I, see text, Figure 4
—	B4	14:02:27.89	54:16:18.43	—	—	Em. Line	—	—	Em. Line; H II region, see text ^c
J140228.83+542014.03	9492_14_14450	14:02:28.83	54:20:14.03	19.74	0.34	Im. SG	$UBVR$	0.9	Early A I; see text ^c , Figure 4
—	V9	14:02:29.92	54:16:19.91	—	—	LBV Cand.	$UBVR$	—	See text, Figure 6
J140248.46+541935.80	9490_c2_14120	14:02:48.46	54:19:35.80	20.10	0.19	Im. SG	—	0.2 – 0.3	Late A I
J140256.71+541834.09	9490_02_152	14:02:56.71	54:18:34.09	20.30	0.20	Im. SG	—	0.2	A5-F0 I
J140259.37+542323.89	9490_a3_10940	14:02:59.37	54:23:23.89	21.49	-0.06	Em. Line	—	0.7 – 0.8	Of/WN; see text, Figure 5
J140301.84+541949.62	9490_02_991	14:03:01.84	54:19:49.62	20.17	0.00	Hot SG	—	0.5	early B-type, weak WN
J140302.61+542001.39	9490_02_1239	14:03:02.61	54:20:01.28	20.02	0.20	Im. SG	—	≈ 0	Early A I
J140304.70+541925.00	9490_02_598	14:03:04.70	54:19:25.00	20.07	0.30	Hot SG	—	1.6	early B I; see text ^c , Figure 3
J140305.13+542342.14	9490_a3_14757	14:03:05.13	54:23:42.14	20.32	-0.03	Hot SG	—	0.3	early B + WN, double emission profiles
J140307.95+542326.81	9490_a3_11594	14:03:07.95	54:23:26.81	21.51	0.06	Hot SG	—	0.8	early B I; see text ^c , Figure 3
J140309.19+542138.77	9490_01_6951	14:03:09.19	54:21:38.77	19.96	0.09	Hot SG	—	0.3	late B; weak WN feature; composite. spectrum
J140311.06+541830.96	9490_a2_20839	14:03:11.06	54:18:30.96	19.95	0.33	Im. SG	V	0.7	A5 I
J140311.32+542518.55	9490_03_6943	14:03:11.32	54:25:18.55	20.18	0.11	Im. SG	—	0.2	early - mid A ^a , see text, Figure 4
J140313.44+541954.44	9490_02_1086	14:03:13.44	54:19:54.44	19.90	-0.02	Hot SG	—	0.1	late B, H em, H β double.
J140313.74+542004.56	9490_02_1340	14:03:13.74	54:20:04.56	20.11	0.28	Im. SG	—	0.3	F0-F2 I; H em.
J140314.80+541737.93	B162	14:03:14.80	54:17:37.93	19.52	0.09	Hot SG	—	0.4	B8 I; see text, Figure 3
J140314.98+541645.26	V4	14:03:14.98	54:16:45.26	22.02	0.05	LBV Cand.	$UBVR$	—	See text, Figure 6
J140316.64+542042.04	9490_01_3663	14:03:16.64	54:20:42.04	21.99	-0.05	Hot SG	—	0.1	B5 I, H β double
J140322.26+542437.69	9490_03_5290	14:03:22.27	54:24:37.62	19.98	0.42	Im. SG	—	0.9	A8 I
J140323.43+542504.84	9490_03_6537	14:03:23.44	54:25:04.76	20.37	0.51	Im. SG	—	1.2	Late A I
J140326.37+542411.63	9490_03_3806	14:03:26.37	54:24:11.63	20.22	0.13	Hot SG	—	0.6 – 0.9	Early B I ^c ; weak WN feature
J140328.35+541707.58	9490_a1_416	14:03:28.35	54:17:07.58	19.90	1.00	Im. SG	—	≈ 1.5	F: I
J140328.86+542128.94	9490_a1_6401	14:03:28.86	54:21:28.94	19.91	0.70	Im. SG	—	1.5 – 1.8	Late A I
J140330.73+542335.77	9490_03_1487	14:03:30.73	54:23:35.66	19.86	0.58	Im. SG	—	1.4	A5 I
—	9490_01_8757	14:03:32.28	54:22:09.19	—	—	Im. SG	V	—	Late F I ^b
J140332.78+542009.89	9490_a1_7093	14:03:32.78	54:20:09.89	20.20	0.31	Hot SG	—	1.3	Mid B: I; see text ^c , Figure 3
J140332.88+542425.99	V2	14:03:32.88	54:24:25.99	20.69	0.13	LBV Cand.	$UBVR$	—	See text ^c , Figure 6
J140341.18+541905.30	9490_b1_3762	14:03:41.18	54:19:05.30	22.13	0.23	Em. Line	—	—	Strong WN feature, see text ^c

^aThe residual [O I] night sky lines in the red appear to have P Cygni profiles due to poor sky subtraction.

^bThe nebular [N II] and [S II] lines appear to have have P Cygni profiles due to poor background/sky subtraction.

^cDouble or split emission lines.

Table 2. Foreground Stars

Catalog ID	Star ID	α_{J2000}	δ_{J2000}	V	$(B - V)$	Variability	Spectral Type
—	9492_12_5654	14:02:23.33	54:28:01.68	—	—	<i>UB</i>	M4 V
—	9490_c2_12822	14:02:39.23	54:19:16.83	—	—	<i>UBVR</i>	K7 V
J140243.90+541727.85	B53	14:02:43.90	54:17:27.85	21.30	0.58	—	F0-F2 III
J140247.62+541728.90	9490_c2_1281	14:02:47.62	54:17:28.90	19.87	0.43	—	Late-A
J140247.76+542833.56	9492_09_25840	14:02:47.76	54:28:33.56	19.91	0.57	<i>U</i>	F8 III/V
—	9492_09_27729	14:02:48.88	54:28:48.76	—	—	<i>UBVR</i>	M2 V
J140250.09+542138.09	9490_02_2795	14:02:50.09	54:21:38.05	20.11	0.76	<i>R</i>	G8 V
J140301.20+541839.71	B65	14:03:01.20	54:18:39.71	18.96	0.31	—	Late A III
J140310.60+541809.18	9490_a2_17826	14:03:10.60	54:18:09.18	22.45	0.47	—	A3 V (WD)
J140312.62+542056.72	9490_01_4552	14:03:12.62	54:20:56.72	19.56	0.34	—	F2 III
J140318.13+542400.97	9490_03_3062	14:03:18.13	54:24:00.97	19.04	0.69	—	G5 V
—	9490_01_4409	14:03:31.38	54:20:53.67	—	—	—	G4 V
J140335.25+542242.89	9490_c1_3304	14:03:35.25	54:22:42.89	22.10	1.60	<i>U</i>	M5 V
—	9490_b2_21	14:03:36.93	54:14:18.72	—	—	—	F8 V
J140342.55+541740.49	9490_a1_1828	14:03:42.55	54:17:40.49	19.03	0.79	<i>BV</i>	F8 V
—	9490_c1_1056	14:03:49.06	54:21:49.73	—	—	<i>BVR</i>	M2 V
—	9490_c1_3679	14:03:49.62	54:23:08.74	—	—	<i>U</i>	M0 V
—	9490_b1_11450	14:03:55.82	54:20:58.20	—	—	—	M4 V
J140356.08+542149.39	9490_c1_1033	14:03:56.08	54:21:49.32	19.08	0.90	<i>B</i>	G8 V

Note. — Spectroscopic targets observed with Hectospec on the MMT. Units of right ascension are hours, minutes, and seconds; units of declination are degrees, minutes, and seconds. Sources are sorted by increasing RA. The *HST*/ACS magnitudes, for recovered sources, are provided.

Table 3. Remaining Targets

Catalog ID	Star ID	α_{J2000}	δ_{J2000}	V	$(B - V)$	Variability	LBT/MODS Field
J140219.79+542315.29	9492_13_7415	14:02:19.79	54:23:15.29	20.26	0.16	<i>VR</i>	
J140219.85+542313.67	9492_13_7103	14:02:19.85	54:23:13.67	20.37	0.82	<i>VR</i>	
J140220.43+542313.06	9492_13_6986	14:02:20.43	54:23:13.06	20.48	0.31	<i>BVR</i>	Field 4
J140221.34+542333.72	9492_13_11152	14:02:21.34	54:23:33.72	20.63	1.05	<i>BVR</i>	Field 4
J140225.55+541917.18	9492_14_1816	14:02:25.55	54:19:17.18	20.85	0.15	—	Field 4
J140226.24+541944.04	9492_14_6605	14:02:26.24	54:19:44.04	20.68	0.09	—	Field 4
J140226.53+542335.74	9492_13_11533	14:02:26.53	54:23:35.74	20.23	1.41	<i>UBVR</i>	Field 4
J140226.64+541948.25	9492_14_7655	14:02:26.64	54:19:48.25	20.74	0.08	—	
J140226.75+541945.84	9492_14_7028	14:02:26.75	54:19:45.84	20.54	0.49	—	
J140226.97+541951.38	9492_14_8521	14:02:26.97	54:19:51.38	20.78	0.06	—	
J140227.03+541947.64	9492_14_7490	14:02:27.03	54:19:47.64	21.02	0.01	—	
J140227.68+542619.32	9492_12_961	14:02:27.68	54:26:19.32	20.94	0.20	<i>UBVR</i>	Field 4
J140231.47+542531.44	9492_13_23814	14:02:31.47	54:25:31.44	20.78	0.82	<i>UBVR</i>	
J140232.51+542001.39	9492_14_11163	14:02:32.51	54:20:01.39	20.09	0.47	<i>UBVR</i>	
J140234.99+542416.67	9492_13_17081	14:02:34.99	54:24:16.67	20.53	1.35	<i>UBVR</i>	Field 4
—	9492_14_1739	14:02:39.24	54:19:16.77	—	—	<i>UBVR</i>	
J140248.90+541840.10	9490_c2_10368	14:02:48.90	54:18:40.10	20.74	0.16	—	
J140249.10+541842.08	9490_c2_10564	14:02:49.10	54:18:42.08	20.24	0.13	—	
J140249.39+542359.14	9490_b1_16197	14:02:49.39	54:23:59.14	21.02	0.31	—	Field 3
J140249.83+541924.17	9492_09_3069	14:02:49.83	54:19:24.20	20.88	0.25	—	Field 1
J140250.63+542346.86	9490_a3_15563	14:02:50.63	54:23:46.86	20.63	0.06	—	Field 3
J140251.11+542114.51	9490_03_4663	14:02:51.11	54:21:14.51	20.60	0.49	<i>U</i>	
J140253.82+542319.14	9490_a1_5661	14:02:53.82	54:23:19.14	20.86	-0.04	—	Field 3
J140254.07+541942.89	9490_02_867	14:02:54.07	54:19:42.89	20.73	0.04	<i>U</i>	Field 1
J140256.45+541830.42	9490_a2-SF10	14:02:56.45	54:18:30.42	20.40	0.00	—	Field 1
J140257.81+541750.64	9490_a3_1058	14:02:57.81	54:17:50.64	20.85	0.42	—	Field 1
J140258.34+541656.35	9490_a2_7168	14:02:58.34	54:16:56.35	20.88	0.72	—	Field 1
J140258.67+542242.49	9490_01_7533	14:02:58.67	54:22:42.49	20.77	0.11	—	
	9490_a1_6666	14:02:59.11	54:21:09.22	—	—	<i>VR</i>	
—	9490_a3_21186	14:02:59.99	54:24:36.05	—	—	<i>UBVR</i>	Field 3
J140300.13+542156.52	9490_02_3047	14:03:00.13	54:21:56.52	20.47	0.12	—	
J140301.82+541514.87	9490_a2_39	14:03:01.82	54:15:14.87	20.86	0.51	—	Field 1
J140302.00+542329.58	9492_10-SF89	14:03:02.00	54:23:29.58	20.22	0.18	<i>UBVR</i>	Field 3
J140302.70+542308.88	9492_10-SF162	14:03:02.70	54:23:08.88	21.38	0.92	—	Field 3
J140306.60+541924.56	9490_02_584	14:03:06.60	54:19:24.56	20.68	0.14	—	Field 1
J140306.84+542147.95	9490_02_2905	14:03:06.84	54:21:47.95	19.96	-0.06	—	
J140309.76+542330.52	9490_a3_12519	14:03:09.76	54:23:30.52	20.35	0.03	—	Field 3

Table 3—Continued

Catalog ID	Star ID	α_{J2000}	δ_{J2000}	V	$(B - V)$	Variability	LBT/MODS Field
J140311.11+541623.59	9490_a2-SF112	14:03:11.11	54:16:23.59	21.12	0.05	—	Field 1
J140312.18+542006.40	9490_02_1378	14:03:12.18	54:20:06.40	20.42	0.01	—	
J140312.52+541752.55	9490_a2_15263	14:03:12.52	54:17:52.55	20.92	0.09	—	
J140312.62+541749.85	9490_a2_14783	14:03:12.62	54:17:49.85	20.70	0.20	V	Field 1
J140312.81+541732.17	9490_a2_12011	14:03:12.81	54:17:32.17	20.84	0.13	—	
J140315.13+542151.19	9490_01_7652	14:03:15.13	54:21:51.19	20.62	0.13	—	Field 3
J140315.66+541907.72	9492_10_5190	14:03:15.66	54:19:07.72	21.30	-0.01	—	Field 1
J140316.03+541756.22	9490_a2_15969	14:03:16.03	54:17:56.22	20.28	0.23	U	Field 1
J140317.37+542506.89	9490_03_6586	14:03:17.37	54:25:06.89	20.47	1.34	U	Field 3
J140317.62+542332.53	9490_03-SF55	14:03:17.62	54:23:32.53	21.27	0.06	—	Field 3
J140317.99+541712.08	9490_a2_9284	14:03:17.99	54:17:12.02	21.29	0.00	—	Field 1
—	9490_a3_4912	14:03:19.25	54:21:49.12	—	—	$UBVR$	Field 3
J140320.92+541705.60	9490_a2_8459	14:03:20.92	54:17:05.60	20.53	0.38	U	
J140321.42+542344.09	9490_03_1988	14:03:21.42	54:23:44.09	20.46	1.26	—	
J140321.81+542346.00	9490_03_2120	14:03:21.81	54:23:46.00	20.31	0.11	—	Field 3
J140323.24+542042.68	9490_a2_17072	14:03:23.24	54:20:42.68	20.82	0.30	—	Field 2
J140324.77+541726.74	9490_a1_1294	14:03:24.77	54:17:26.74	20.90	0.15	—	Field 1
J140325.40+541939.04	9490_a1_6386	14:03:25.40	54:19:39.04	20.59	1.40	BVR	
J140325.45+542522.94	9490_03_7146	14:03:25.45	54:25:22.94	20.66	0.02	V	Field 3
J140325.57+542353.02	9490_03_2492	14:03:25.57	54:23:53.02	20.29	0.64	V	Field 3
J140325.58+541957.65	9490_01_1198	14:03:25.58	54:19:57.60	20.58	0.10	VR	Field 2
J140325.70+542514.88	9490_03_6836	14:03:25.70	54:25:14.88	20.27	0.04	R	Field 3
J140325.90+542420.88	9490_03_4390	14:03:25.90	54:24:20.88	22.61	0.01	—	Field 3
J140325.98+542422.82	9490_03_4520	14:03:25.98	54:24:22.82	20.02	0.41	—	
J140326.19+541939.47	9490_c1_1362	14:03:26.19	54:19:39.47	20.81	0.66	—	Field 2
J140326.21+542047.87	9490_01_4031	14:03:26.21	54:20:47.87	20.67	0.01	U	
J140326.38+542411.30	9490_02_2637	14:03:26.38	54:24:11.30	20.69	-0.04	—	Field 3
J140326.45+542038.36	9490_01_3379	14:03:26.45	54:20:38.36	20.65	0.07	—	
J140327.03+542346.36	9490_03_2142	14:03:27.03	54:23:46.36	21.08	-0.06	—	
J140327.10+542046.79	9490_01_3977	14:03:27.10	54:20:46.79	20.82	0.09	—	Field 2
J140327.60+541846.80	9490_a1_4198	14:03:27.60	54:18:46.80	20.75	0.01	—	
J140327.67+542340.92	9490_03_1822	14:03:27.67	54:23:40.92	19.69	0.40	—	
J140327.71+541844.93	9490_a1_4062	14:03:27.71	54:18:44.93	20.89	0.05	—	
J140328.82+542458.03	9490_03_6315	14:03:28.82	54:24:58.03	20.15	0.84	U	
J140329.43+541809.97	9490_a3_7830	14:03:29.43	54:18:09.97	20.54	0.25	—	
J140329.51+541712.23	9490_a1_627	14:03:29.51	54:17:12.23	20.81	0.19	—	
J140330.07+541853.28	9490_c1_1485	14:03:30.07	54:18:53.28	20.52	0.30	U	Field 2

Table 3—Continued

Catalog ID	Star ID	α_{J2000}	δ_{J2000}	V	$(B - V)$	Variability	LBT/MODS Field
J140330.32+541954.19	9490_01_991	14:03:30.32	54:19:54.19	20.80	-0.06	—	
J140330.61+542424.48	9490_c2_2831	14:03:30.61	54:24:24.48	20.45	0.77	<i>UV</i>	Field 3
—	9490_b2_14	14:03:30.91	54:14:10.48	—	—	—	
—	9490_b1_14323	14:03:32.13	54:22:00.47	—	—	—	Field 2
J140333.74+541854.61	9490_a1_4710	14:03:33.74	54:18:54.61	20.57	0.48	—	Field 2
—	9490_b1_3388	14:03:40.92	54:19:02.68	—	—	—	Field 2
—	9490_03_3779	14:03:41.57	54:19:08.47	—	—	<i>UB</i>	
J140342.85+542336.96	9490_c1_4050	14:03:42.85	54:23:36.96	20.65	0.20	<i>UBV</i>	
J140346.10+541959.52	9490_b1_8183	14:03:46.10	54:19:59.52	20.77	0.07	—	Field 2
—	9490_c1_1535	14:03:46.17	54:16:15.68	—	—	<i>UBVR</i>	
—	9490_c1_3069	14:03:47.38	54:22:29.50	—	—	<i>UBVR</i>	
—	9490_c1_3679	14:03:49.63	54:23:8.74	—	—	<i>BV</i>	
J140351.93+542152.78	9490_c1_1292	14:03:51.93	54:21:52.78	20.33	-0.02	—	
J140355.88+542229.46	9490_c1_3067	14:03:55.88	54:22:29.46	20.30	0.11	—	